https://doi.org/10.5194/egusphere-2026-2102
Preprint. Discussion started: 27 April 2026

Seasonal variation of the size distributions of black carbon in the Arctic

John Backman[1], Sho Ohata[2], Yutaka Kondo[3], Jonas Svensson[1], Eija Asmi[1], Hitoshi Matsui[4], and Tatsuhiro Mori[5]

[1]Atmospheric Composition Research, Finnish Meteorological Institute, Helsinki, FI-00560, Finland

[2]Institute for Space–Earth Environmental Research (ISEE), Nagoya University, Nagoya, Aichi, Japan

[3]Professor Emeritus, The University of Tokyo, Tokyo, Japan

[4] Graduate School of Environmental Studies, Nagoya University, Nagoya, Aichi, Japan

[5]Department of Applied Chemistry, Faculty of Science and Technology, Keio University, Yokohama, Kanagawa, Japan

Correspondence to: John Backman (john.backman@fmi.fi)

Abstract. Black carbon (BC) aerosol particles strongly absorb solar radiation and heat the atmosphere. BC aerosols also deposit on snow and ice, lowering the surface albedo and accelerate heating of the Arctic. Because these BC radiative effects are size-dependent, an improved understanding of BC size distributions is indispensable for radiative transfer modelling to estimate the aerosol climate effects. We measured BC size distributions at Pallas, northern Finland, for the first time throughout the whole year, to fully capture its seasonal variability connected with the BC atmospheric processing during transport. The shape of the size distribution was very stable, with little seasonal variation. Comparison to previous seasonal observations at Ny-Ålesund in Svalbard, Norway, and Alert in Canada confirmed very similar size distribution shapes at all three sites, suggesting minor spatial variability. Strong temporal variations were observed in the total mass concentration of BC, but not in the shape of the BC core size distributions. The results were additionally used for validation of the state-of-the-art global climate model CAM5-ATRAS monthly BC size at Pallas. Overall, our observational results

https://doi.org/10.5194/egusphere-2026-2102
Preprint. Discussion started: 27 April 2026

provide useful constraints for estimating the effects of BC on climate by model simulations, especially in the Arctic, where the measurements were conducted.

1 Introduction

Black carbon (BC) aerosols are produced by the incomplete combustion of carbon-based fuels and play a key role in the Arctic radiation budget because of their strong light-absorbing properties (AMAP 2021; Bond et al., 2013; Oshima et al., 2020; Sand et al., 2015). The Arctic is a particularly vulnerable region that is warming at four times the rate of the rest of the world (Rantanen et al., 2022). The impact of BC on climate strongly depends on its mass concentration (M_{BC}) and microphysical properties, including size distribution and mixing state, all of which affect light absorption (Matsui et al., 2018, 2022). At their emission source, BC particles are typically fractal-like with a monomer diameter of 10–50 nm (Adachi et al., 2010), after which they undergo atmospheric aging and gain a coating and/or mix with other aerosol components (Jacobson, 2001; Whaley et al., 2022). Atmospheric aging of BC can be as fast as 3 h, and aging time scales in model representations are important for BC concentrations in the Arctic (Fierce et al, 2025). When aged BC is cloud activated, the fractal-like structure of fresh BC will collapse (Mikhailov et al., 2006). Moreover, a non-absorbing coating around the BC can substantially enhance aerosol light absorption (Bond et al., 2006). Climate impacts of BC on the Arctic are best studied by models, but those models need to rely on accurate and plentiful measurements in order to be accurate; including process-based studies and long-term measurements from a variety of settings.

The dominant sources of spread across models in simulations of Arctic BC have evolved across successive generations of atmospheric models, with each generation improving upon the last. The spread between early generation models largely stemmed in a diversity of emission inventories and overly simplified removal processes, both leading to a large variability in BC mass concentrations and lifetime (Koch et al., 2009). In subsequent model generations, with harmonized emissions, the spread has been attributed to uncertainties in wet scavenging parameterizations and vertical transport, with wet removal being the likely dominant factor for Arctic BC mass concentrations (Eckhardt et al., 2015). Arctic BC modelling studies looking at BC source attributions have shown that

https://doi.org/10.5194/egusphere-2026-2102
Preprint. Discussion started: 27 April 2026

discrepancies arise from interactions between emissions, transport pathways, and removal processes, leading to persistent biases in the seasonal cycle and regional contributions (Zhao et al., 2021). In the most recent generation of Earth system models, including those assessed in Whaley et al. (2022) and the AMAP 2021 assessment, inter-model variability of Arctic BC mass concentrations has narrowed, but there are still substantial uncertainties in the BC radiative forcing. This uncertainty is primarily linked to deficiencies in the representation of mixed-phase cloud scavenging, BC mixing state and associated absorption enhancement, vertical distribution biases, and poorly constrained snow–ice deposition and post-depositional processes. The above studies jointly point towards a shift from emission-driven uncertainties in early models toward process-level uncertainties and understanding, even on a particle-by-particle basis (Fierce et al., 2025). To address the remaining uncertainties, detailed understanding about the microphysical properties of BC is the key.

Observations of the specific microphysical properties of BC have increased with the development of new instrumentation. For example, BC size distributions can be measured using a single-particle soot photometer (SP2). Compared with instruments that provide the bulk BC mass or absorption properties, SP2 requires more complex maintenance and collects greater amounts of data. To date, SP2 has mainly been used for short-term field campaigns in the Arctic, although it provides unparalleled precision and detail regarding BC size distributions and mass concentration.

Ground-based measurements of BC size distributions have been conducted at Ny-Ålesund (spring) and Alert (spring and summer) (Ohata et al., 2019, 2021b). At the Pallas GAW Arctic super-site in Finland, Raatikainen et al. (2015) observed during a 3-month winter measurement campaign that the BC mass was log-normally distributed, showing a relatively constant BC core mass median diameter with an average of 194 nm, typical for aged air masses. One long-term BC size distribution study has been conducted at Alert (Sharma et al., 2017). Although the focus was on evaluating three different methods for measuring BC, the authors also reported in their seasonal averages for size distributions for four seasons based on log-normal fits to a narrow size range. When utilized in aircraft campaigns, SP2 measurements has covered great aerial extents, yet on very short time-scales, stable BC size distributions have been observed (Jurányi et al., 2023).

https://doi.org/10.5194/egusphere-2026-2102
Preprint. Discussion started: 27 April 2026

Because the greater majority of studies investigating the microphysical properties of BC have been brief, our main goal is to provide a novel dataset to fill this observational gap. Our aims are to evaluate the BC temporal and spatial variability in the Arctic with a one year measurement campaign at Pallas and to put this into a greater context by providing a first full-year validation of the global CAM5-ATRAS model BC size output. The structure of this study is as follows: first the long-term stability of BC mass concentration measurements using SP2 by comparing it with another long-term BC instrument (COSMOS) is evaluated (Section 3.1); second, the seasonal variation of BC size distribution is studied in detail and the impact of different atmospheric conditions (Section 3.2); third, our results from Pallas are compared with other Arctic results and study BC size spatial variability (Section 3.3); and lastly, our observational data is used as a ground-truth to validate the simulated BC size distributions from CAM5-ATRAS model, resolving the mixing state of BC and models BC size distribution (Section 3.4). In brief, our results essentially contribute to reducing the current uncertainties in BC size distribution variability in the Arctic.

2. Methods

2.1 Measurement sites

2.1.1 Long term measurement site Pallas

All measurements were performed at the research station of the Finnish Meteorological Institute in Pallas, in the Finnish Arctic (68.0°N, 24.1°E). The main station building is located on top of the Sammaltunturi fell, at a height of 565 m above mean sea level (amsl). A detailed description of the Pallas Sammaltunturi measurement site is provided elsewhere (Hatakka et al., 2003).

At Pallas, the SP2 measured BC through a total aerosol inlet, which is essentially a hood through which sample air is drawn into the station and instruments. The sample air was dried using a Nafion membrane dryer before entering the SP2. The inlet is described in more detail elsewhere (Backman et al., 2025). In addition, the filter-based absorption photometer (COSMOS) also sampled through the total aerosol inlet. The

https://doi.org/10.5194/egusphere-2026-2102
Preprint. Discussion started: 27 April 2026

COSMOS had a 1-µm inline cyclone, whereas the SP2 sampled directly from the total inlet.

Measurements were conducted by the SP2 between 29 November 2019 and 16 December 2020. COSMOS has been running continuously at the Pallas station since summer 2019. The concentrations presented in this study are reported at standard temperature (0 °C) and pressure (1013 hPa).

2.1.2 Spring and summer campaigns at Alert and Ny-Ålesund

In addition to Pallas, where the long-term SP2 measurements were conducted, previous data from Alert (Canada) and Ny-Ålesund (Svalbard) were also included in this study for comparison. The Ny-Ålesund measurement station is located at 78.9°N, 11.9°E on Zeppelin mountain, at an altitude of 475 m amsl. The station is maintained by the Norwegian Polar Institute. The Alert measurement station in the Canadian Arctic is located at 82.5°N, 62.5°W, at an altitude of 8 m amsl (Sharma et al., 2017). The station is operated by the Environment and Climate Change Canada (ECCC). The locations of these sites are shown in Figure 1.

The measurements were conducted in Alert from January to May 2018, with the SP2 connected to a total aerosol inlet with a 1-µm inline cyclone. A more detailed description of the measurement setup and station is outlined in (Ohata et al., 2021b; Sharma et al., 2017). The SP2 measurements at Ny-Ålesund, , were conducted from February to March 2017,.sampled through a total air inlet. The measurements and site are described in more detail elsewhere (Ohata et al., 2019).

2.2 Instruments

2.2.1 SP2

The SP2 (Droplet Measurement Technologies. Longmont, CO; USA) uses a continuous high power intracavity infrared (IR) laser to heat BC containing particles to the point of incandescence (Baumgardner, 2004; Schwarz et al., 2006; Stephens et al., 2003). The SP2 was calibrated using fullerene soot (Gysel et al., 2011; Laborde et al., 2012). A limiting factor for long-term SP2 measurements is often the vast amounts of

https://doi.org/10.5194/egusphere-2026-2102
Preprint. Discussion started: 27 April 2026

data gathered and the computational expense required for analysis. Owing to the vast amounts of data collected, the data were analysed on a supercomputer using the pysp2 (version 1.5) software package (https://github.com/ARM-DOE/PySP2).

In this work, we used the broadband channel that detects incandescent light in the wavelength range of 350 – 800 nm, which is the most sensitive to BC (Laborde et al., 2012). Due to the low number concentrations at Pallas, we did not apply the deadtime correction scheme, as the correction for such low concentrations was deemed unnecessary (Schwarz et al., 2022). The maximum number of incandescence particles was 301 cm^{-3} (mean 5.8 cm^{-3}) and the maximum number of scattering particles was 893 cm^{-3} (mean 66 cm^{-3}). Therefore, the deadtime correction would not exceed 0.4%.

Previous studies have demonstrated that the SP2 incandescence detector is stable over time when the instrument is not moved or the optics are not contaminated (Schwarz et al., 2010a). The mass of individual BC particles measured by SP2 was converted to the equivalent particle diameter (D), assuming a spherical shape and a constant density (ρ) of 1.8 g cm^{-3}. The diameter range measured by the SP2 was 65 – 537 nm.

The detection of BC by SP2 is referred to as refractory BC (rBC), whereas filter-based absorption photometers measure equivalent BC (eBC) (Petzold et al., 2013). In this work, the specific measurement-based terminology was omitted for simplicity and cohesion in the text, although it is important to note this difference. For mass concentrations of BC from SP2 and COSMOS, we used M_{BC}; however, we distinguished from which instrument the M_{BC} values were reported.

2.2.2 COSMOS

COSMOS (Kanomax, Osaka, Japan) is a filter-based absorption photometer designed for long-term, unattended monitoring of M_{BC} (Kondo, 2015; Miyazaki et al., 2008; Mori et al., 2025; Ohata et al., 2019). A special feature of COSMOS compared to other filter-based absorption photometers is that it is operated behind a heated inlet (300 °C) to volatilize light-scattering species (externally and internally mixed with BC) from the aerosol particle phase. For sub-micron aerosol particles, this temperature is sufficient to volatilize much of the light-scattering constituents, which greatly reduces the instrument's cross-sensitivity to other aerosol constituents than BC. Simultaneous measurements of M_{BC} by COSMOS and SP2 for up to a few months in Asia and in the

https://doi.org/10.5194/egusphere-2026-2102
Preprint. Discussion started: 27 April 2026

Arctic agreed to within 10–15 % (Kondo et al., 2009, 2011; Ohata et al., 2019). To prevent the impact of non-volatile particles larger than 1 μm in diameter, COSMOS was sampling behind a PM_1 cyclone.

2.3 Model simulations

To further analyse the observed BC size distributions, global aerosol simulations were performed using the CAM5-ATRAS model (Matsui, 2017; Matsui and Mahowald, 2017). This study utilized the same model outputs as those in (Matsui et al., 2022), specifically the modelled BC size distributions. CAM5-ATRAS includes essential processes, such as emissions, gas-phase chemistry, new particle formation, condensation and evaporation, coagulation, aqueous-phase chemistry, dry and wet deposition, and interactions with radiation and clouds. The model addresses seven aerosol species (sulphate, nitrate, ammonium, dust, sea salt, organic aerosol, and BC). These species are modelled using a two-dimensional sectional approach. The model divides dry particle diameters into 12 size bins ranging from 1 nm to 10 μm. BC mixing states for fine particles are modelled in eight bins ranging from 40 nm to 1.25 μm. Due to these eight bins, the mass mean diameter (MmD) offers better statistics of the modelled BC aerosol size distribution than the mass median diameter (MMD). Consequently, the model results are reported as MmD and compared with the MmD of the measurements. The CMD of the BC emissions in the model for fossil fuel and biomass burning is 70 and 100 nm, respectively, with a σ_c of 1.8. This corresponds to an MMD of 197 nm for fossil fuel emissions and 281 nm for biomass burning emissions, which will be discussed later. The analysis is based on model simulations covering the period 2009–2015, with a horizontal resolution of 1.9° × 2.5° latitude/longitude and 30 vertical layers. Meteorological conditions were adjusted for temperature and horizontal wind fields in the free troposphere based on the Modern-Era Retrospective analysis for Research and Applications version 2 (MERRA2) dataset. Monthly anthropogenic emissions were sourced from the CMIP6 inventory (Hoesly et al., 2018). Daily biomass burning emissions were obtained from the Global Fire Emissions Database version 4.1 (van der Werf et al., 2017).

3. Results

https://doi.org/10.5194/egusphere-2026-2102
Preprint. Discussion started: 27 April 2026

3.1 BC mass concentration

Previous research has shown that the SP2 is stable for periods of months (Schwarz et al., 2010b); however, long-term (>1 year) stability in ambient measurements has not yet been demonstrated. Therefore, before analysing the observed size distribution of BC in greater detail, we investigated the stability of the SP2 by comparing the M_{BC} (SP2) with the M_{BC} measured by COSMOS, hereafter denoted as M_{BC} (COSMOS). COSMOS was selected as a reference instrument because its accuracy and stability have been widely demonstrated in previous publications (Ohata et al., 2019).

The time series of the 1-h averaged M_{BC} (SP2) and M_{BC} (COSMOS), shown in Figure 2, confirms excellent data coverage from both instruments: SP2 data were available 97% of the time, and COSMOS data were available 93% of the time. To the authors' knowledge, this is the longest time series of concurrent SP2 and COSMOS measurements that have been conducted and reported in the literature. The average M_{BC} (SP2) and M_{BC} (COSMOS) were calculated for the overlapping period of measurements and were 17.5 and 18.1 ng m^{-3}, respectively.

Figure 3 shows the linear correlation between the hourly averaged M_{BC} (SP2) and M_{BC} (COSMOS) data. The slope of the fit, forced through zero, was 0.94, and the Pearson's correlation coefficient (r^2) was 0.981, demonstrating the stability of the SP2 instrument. This held true for over a year of measurements, when the SP2 was operated in a stable and controlled environment without moving it after installation.

The particle size distribution of BC can be characterized using log-normal function fits. The particle mass size distribution $n_m(D)$ is expressed as a log-normal function,

$$n_m(D) = \frac{dM}{d\log(D)} = \frac{M_{BC}}{2\pi^{1/2}\log(\sigma_m)} \exp\left(-\frac{\log(D)-\log(MMD)}{2\log^2(\sigma_m)}\right) (1)$$

where M_{BC}, MMD, and σ_m are the total BC mass concentration, mass median diameter, and geometrical standard deviation, respectively. Similarly, the number size distribution, n_n (D), is expressed using the total number concentration (N), count median diameter (CMD), and geometric standard deviation σ_c.

Normalized number size distributions are defined as

https://doi.org/10.5194/egusphere-2026-2102
Preprint. Discussion started: 27 April 2026

$$R_{\mathrm{n}}(D) = n_{\mathrm{n}}(\mathrm{D})/N \quad (2)$$

, and normalized mass size distribution as

$$R_{\mathrm{m}}(D) = n_{\mathrm{m}}(\mathrm{D})/M_{\mathrm{BC}}. \quad (3)$$

Figure 4 shows the mean BC number and mass size distributions measured at Pallas and the fitted log-normal distribution functions $n_{\mathrm{n}}(D)$ and $n_{\mathrm{m}}(D)$. For the unimodal size and mass distribution, the calculated CMD and MMD were 99 nm and 195 nm, respectively, with corresponding σ values (σ_{c} and σ_{m}) of 1.57 and 1.66. This is consistent with earlier SP2 results from Pallas done between 17 December 2011 and 2 February 2012, where the calculated MMD was 194 nm with a σ_{m} of 1.70 (Raatikainen et al., 2015). This also suggests that the modal shape of the BC size distribution remains fairly constant throughout the years. Raatikainen et al., (2015) also showed that the BC at Pallas was systematically aged, i.e. that the BC had a significant coating (core-to-shell ratio of 2.0 in the BC size range of 150 – 200 nm) and no bare BC particles were detected.

The SP2 upper detection range is limited to 537 nm, as shown in Fig. 4; therefore, the entire BC size distribution is not captured by the SP2. A typical method to correct for the missing mass is by using log-normal fitting (Sharma et al., 2017; Zanatta et al., 2018). By fitting two $n_{\mathrm{m}}(D)$ to the data, as shown in Fig. 4, the total M_{BC} of the BC mass distribution can be estimated above the detection limit of the SP2. Here, log-normal fits were done using the method described by (Hussein et al., 2005), which we modified to work with BC mass distributions. With two $n_{\mathrm{m}}(D)$ fits to the data, where the first mode peaks at 187 nm (σ_{m}=1.60) and the second mode at 475 nm (σ_{m}=1.73), we obtained a BC distribution for the size range of 10 to 1000 nm (Figure 4). The BC mass integrated from this fitted bi-modal distribution is hereafter called M_{BC} (SP2 corrected). The goodness of the fit required data averaging and after careful sensitivity tests we selected 12-h averaging interval which led to sufficiently stable fitting results. Due to this practical limitation, the M_{BC} (SP2 corrected) data is only available at 12-h time resolution. However, correcting for the missing mass clearly increased the BC mass concentrations: The mean M_{BC} (SP2) concentration for the whole period of SP2 measurements was 14.9 ng m^{-3} which increased

https://doi.org/10.5194/egusphere-2026-2102
Preprint. Discussion started: 27 April 2026

to 15.7 ng m^{-3} for M_{BC} (SP2 corrected). M_{BC} (SP2 corrected) is thus 5.1% greater than the uncorrected BC mass in the size range of 65 – 537 nm.

The missing BC mass in SP2 offers a logical explanation for the discrepancy between SP2 and COSMOS measured mass concentrations discussed earlier (Figure 3). Therefore, we repeated the linear regression analysis using 12-h averaged M_{BC} (SP2-corrected) and M_{BC} (COSMOS) data, in which the slope increased to 0.955 and r^2 decreased to 0.971. The decreasing time resolution of the data could affect the lower correlation coefficient (sample size) while reducing data noise and improving the regression.

3.2 Seasonal and in-cloud variation of BC size distribution at Pallas

Figure 5 shows that although the BC number (Fig 5a) and mass (Fig 5b) concentrations change throughout the year, the shape of the BC size distribution remains highly stable (Figure 5c). The 12-h average MMD for the entire period was 194 ± 20 nm.

To investigate the variability of the BC size distribution, we normalized the mass and number distributions, $R_m(D)$ and $R_n(D)$, respectively, observed at Pallas. Figures 6a and 6b show the monthly mean $R_m(D)$ and $R_n(D)$, and the monthly average CMD and MMD of the distributions are summarized in Table 1, along with their σ_m. A key observation is the similarity of the distributions. The month of January deviates the most, which is associated with a somewhat larger MMD of 235 nm than the rest of the winter months, in which the MMD was approximately 200 nm (Fig 6a). In contrast, the smallest MMD was measured in September (178 nm). Excluding January and September, the monthly mean MMD during the year varied between 185 and 201 nm.

The 12-h average CMD and MMD throughout the year were 95 ± 9 nm and 194 ± 20 nm, respectively. For hourly averaged data, the results were virtually the same, with mean CMD and MMD values of 95±11 nm and 198±35 nm, respectively. Overall, these results demonstrate that both $R_n(D)$ and $R_m(D)$ show very little seasonal variation at Pallas. The Pallas station, at an elevation of 565 m, can be inside low-level clouds for extended periods, especially from September to November. At other times the station is below the clouds, if there are any. The station is frequently used for aerosol in-cloud characterization (Doulgeris et al., 2025), and here enabled us to study implications of cloud processing on the observed BC size distributions.

https://doi.org/10.5194/egusphere-2026-2102
Preprint. Discussion started: 27 April 2026

The SP2 data from Pallas were separated into three categories: when the station was inside a cloud (visibility below 500 m), good visibility (visibility above 10 km), and when it was raining. For this, we used the station's Vaisala FD12P weather sensor. The resulting categories comprise 1837 h of in-cloud data, 5593 h of good visibility, and 1008 h of data when it was raining. The total SP2 dataset comprised 8938 h of data; therefore, the station was in the cloud 20% of the time.

Figure 7 shows the mean BC size distributions for the three different conditions. The BC mass size distribution shape is not impacted by the presence of clouds nor rain, and the mode remains around 200 nm suggesting that clouds have little to no impact on the shape of the BC size distribution.

3.3 BC size distribution spatial variability in the Arctic

We compared our results with earlier seasonal SP2 measurements conducted in Alert, Canada, and Ny-Ålesund, Svalbard. Figures 8a and 8b show a comparison of $R_m(D)$ and $R_n(D)$ measured at Alert and Ny-Ålesund with the average size distribution measured at Pallas. Both the Ny-Ålesund and Alert measurements were conducted during Arctic winter and spring. The SP2 measurements at Alert were conducted from January to May 2018 (Ohata et al., 2021b), whereas the Ny-Ålesund measurements were conducted during February and March in 2017 (Ohata et al., 2019). Winter and spring in the high Arctic are associated with elevated concentrations of atmospheric pollutants from long-range transport, also known as the Arctic haze period (Quinn et al., 2007). This holds true for both Alert and Ny-Ålesund, whereas Pallas has more variable seasonal influences (Schmeisser et al., 2018). However, both $R_n(D)$ and $R_m(D)$ from Alert and Ny-Ålesund spring and winter measurements are similar to those observed at Pallas throughout the year.

The mean of all campaign BC size distribution data at Ny-Ålesund resulted in an MMD of 228 nm (σ_m=1.74, M_{BC}=27.0 ng m^{-3}), whereas the MMD at Alert was 216 nm (σ_m=1.73, 18.9 ng m^{-3}). For Pallas, the MMD for the entire year was 194 ± 20 nm (σ_m=1.66, M_{BC}=14.9 ng m^{-3}). For the winter months (December to February), the MMD was 209 nm (σ_m = 1.66, M_{BC}=15.8 ng m^{-3}), whereas in spring (March to May), it was 200 nm (σ_m = 1.63, M_{BC}=13.1 ng m^{-3}). Given that these three measurements are not from the

https://doi.org/10.5194/egusphere-2026-2102
Preprint. Discussion started: 27 April 2026

same year, the shape of the BC size distribution around the Arctic appears very similar and within the narrow variability we observed throughout the year at Pallas from November 2019 to December 2020 (Figures 8a and b).

Although the Alert and Ny-Ålesund measurements were conducted during the Arctic haze period, when concentrations in the Arctic are the highest, the observed BC size distributions are similar to those observed at Pallas year-round. This implies that the season is not critical for the comparison. This further implies that the amount of M_{BC} in the lower tropospheric Arctic air is not dictated by the size distribution of BC, but rather by the total number of BC particles which have very homogeneous properties; the MMD close to 200 nm and a small variability in σ_m, as discussed above, and which are all very similar regardless of the season, year, and site.

3.4 Comparison to simulated BC size distributions

Our key result on the seasonal stability of Arctic BC size is useful for both validating and constraining global models, which will be demonstrated here. In the Arctic, the models generally have difficulty replicating the seasonal M_{BC} concentrations (Whaley et al., 2022). Moreover, most models do not include realistic representation of BC size and mixing state in the level of detail needed to estimate its climate impacts (Fierce et al., 2025, Matsui et al., 2018).

The global climate–aerosol model CAM5-ATRAS can provide the BC size, which we validated using the monthly measured BC size observations at Pallas. The simulations covered the period 2009–2015, as described by (Matsui et al., 2022)., and therefore represent typical Arctic BC characteristics, rather conditions over a particular month or year. To date, the CAM5-ATRAS model BC size has not been validated with a whole year of ambient data.

A comparison of the simulated and measured mass mean diameters (MmD) at Pallas is shown in Figure 9 and in Table 1, along with the MMD from the ambient SP2 measurements at Pallas. Both the modelled and measured MmD values cover the same size range (65 – 537 nm) and are in this respect directly comparable.

The modelled MmD of BC at Pallas was 175 ± 4 nm, which is approximately 20% lower than the measured monthly mean value of 219 ± 10 nm (including all data) or 19% lower than 216 ± 6 nm (excluding January as an outlier).

https://doi.org/10.5194/egusphere-2026-2102
Preprint. Discussion started: 27 April 2026

The monthly variation of the modelled MmD was 7%, compared with 21% for the measured MmD. If January (as an outlier month) is excluded, the variation in the MmD measured at Pallas becomes only 10%. Excluding January as an outlier is warranted because the measurement and modelled periods do not overlap.

The stable BC size provided by the model suggests that Arctic air masses have already undergone substantial atmospheric aging during long-range transport from major sources located at lower latitudes. BC concentrations are low in the Arctic, and the particle removal processes, such as wet and dry deposition and scavenging, have removed a substantial amount of BC aerosols during long-range transport (Stohl, 2006). This minor temporal variability is supported by our observations, although the modelled MmD absolute values are biased low by 10% to 25%, depending on the month. Given the complexity of modelling Arctic BC sources and processes (Matsui et al., 2018; Whaley et al., 2022), the obtained overall agreement is encouraging and can help to evaluate the uncertainties in modelling the BC climate impacts in the Arctic.

4 Discussion

Our deduction on the stability of BC size are supported by BC measurements from multiple aircraft campaigns carrying SP2 (Jurányi et al., 2023). BC aerosol size distributions have been conducted onboard aircraft in the Arctic to investigate profiles and transects of BC properties (Jurányi et al., 2023; Ohata et al., 2021a; Schulz et al., 2019; Zanatta et al., 2023). These aircraft campaigns were conducted during spring and summer in 2009, 2011, 2013, 2014, 2015, 2017, and 2018. To the authors' knowledge, aircraft campaigns in the autumn and winter seasons in the Arctic have not been reported in the literature. An overview of the 2009 - 2017 aircraft campaigns are presented by (Jurányi et al., 2023) and 2018 in (Ohata et al., 2021a).

These aircraft campaigns comprise the PAMARCMiP 2009, 2011, 2013, 2017, 2018, RACEPAC 2014, NETCARE 2014, 2015, and ACLOUD 2017 projects which all had SP2 instruments onboard. The area covered by these campaigns is around Svalbard, northern Greenland, and the Canadian high Arctic totalling 187 flight hours and covering two seasons and a vast portion of the Arctic. The conclusion was that there is no significant difference in the average BC size or in the shape of the size distribution between the two seasons in the area covered by the campaigns. For all flights and altitudes,

https://doi.org/10.5194/egusphere-2026-2102
Preprint. Discussion started: 27 April 2026

the MmD in spring was 202 nm and in summer 210 nm, although the M_{BC} varies by a factor of four between spring and summer, with lower concentrations in summer (Jurányi et al., 2023). The apparent similarity in our observations with the various vertical observations could indicate that BC vertical gradients in the Arctic are not largely affected by cloud processing.

During the PAMARCMiP 2018 campaign, between Greenland and Svalbard (Fram Straight) in spring 2018, MMD were between 168 to 228 nm, depending on altitude (Ohata et al., 2021a). At the lowest altitude (125 m), the MMD was 228 nm (σ_m = 1.76). The MMD decreased with altitude and was the smallest 168 nm (σ_m = 1.63) at 5000 m, which was the highest altitude of that aircraft campaign. During the 2009 – 2017 flight campaigns, covering a much greater area both spatially and temporally, similar results were obtained from combining all the flight data. In spring, at the lowest altitude < 500 m, the MmD was 214 nm and decreased with altitude at a rate of -5.3 nm km^{-1} to reach 194 nm between 3500 – 4000 m of altitude (Jurányi et al., 2023). In summer, there was little difference, only 5 nm, between MmD the lowest and (< 500 m) highest altitudes (3500 – 4000 m). In summary, the Aircraft campaigns from 2009 – 2017 in spring and summer, for all altitudes, the MMD was 187 ± 16 nm. This is also very close to what we measured at Pallas for a whole year at Pallas (194 ± 20 nm). The study by Jurányi et al., (2023) does not report the MMD for the aircraft data for the lowest flight levels. The lowest flight level would be the best comparison altitude between the aircraft data and the Pallas data.

The aircraft campaigns discussed above also found lofted layers of high BC concentrations associated with wildfire smoke, at altitudes of 3000 m or more. These smoke plumes were associated with MMD above what we measured at ground level, about 240 nm in biomass burning plumes. It is intriguing that the spring aircraft campaigns showed a decrease in MMD and MmD with altitude (except in smoke plumes), where the biggest particles were found at ground level, and the smallest MMD at 4000 m in altitude, or more.

We could also identify the BC size distribution shape in cloudy and rainy conditions. Cloud processing of aerosols can alter the BC size distributions, as discussed by Zanatta et al. (2023)They found that BC size distributions below and inside Arctic clouds are

https://doi.org/10.5194/egusphere-2026-2102
Preprint. Discussion started: 27 April 2026

associated with a higher abundance of large BC particles compared to above clouds and clear-sky conditions, detected as a shoulder on the BC size distribution above the main mode of the size distribution (see Zanatta et al. 2023 Fig. 3a and 3b). Their work was based on an aircraft campaign around Svalbard in summer 2017. At Pallas, we do not see a clear shoulder in any season during the station in-cloud episodes (Fig. 7), indicating that the low-level clouds at Pallas did not change the BC size distribution substantially. We hypothesize that the aerosol in Pallas was already highly aged and cloud-processed, for which any further impact was not observed. The differences in cloud altitude and type between Pallas and Zanatta et al., 2023 observations can also explain part of the discrepancy.

5 Conclusions

The large-scale climate impacts of BC are studied using models. The developments in this area have increasingly been focusing on process-level uncertainties such as cloud microphysics and aerosol-radiation interactions. Uncertainties in the representation of mixed-phase cloud scavenging, BC mixing state and associated absorption enhancement, vertical profile biases, and deposition onto snow and ice, and post-depositional processes are key ongoing research areas. In addition to observations of vertical profiles, BC size distributions are key constraints to advance these research areas. Our unique long-term observational results imply that Arctic BC size distributions do not wary substantially in space nor time. M_{BC} can vary by orders of magnitude while the MMD of the BC size distribution seems unaffected.

These conclusions on the mass and size distributions of individual BC particles were based on measurements by single-particle soot photometer (SP2) continuously for over a year at Pallas station in northern Finland (68°N). The count median diameter (CMD) and mass median diameter (MMD) for the whole period were 95±9 nm and 194±20 nm, respectively.

The Pallas BC size distributions were compared to previous SP2 measurements in Alert (Canada), and in Ny-Ålesund (Svalbard, Norway) during winter and spring seasons. The observed similarity in normalized BC size distribution shapes at these three sites suggests a broadly spatially and temporally uniform BC size distribution over much of the Arctic boundary layer. Our unique measurement set-up also enabled comparison between in-

https://doi.org/10.5194/egusphere-2026-2102
Preprint. Discussion started: 27 April 2026

cloud, precipitation and high visibility BC size distributions. The evident similarity of those supports our main conclusion on a broadly homogenous lower tropospheric BC size distribution persisting in the Arctic. We did not observe substantial evidence of cloud processing of BC particles that would increase the size of the BC cores.

The stability of the BC size distribution shape in the Arctic is supported by previous literature. For example, several aircraft studies around Svalbard, northern Greenland, and the Canadian Arctic between years 2009 and 2017 showed a mean MMD of 187±16 nm - very close to our annual MMD result for Pallas (Jurányi et al., 2023). A MMD ranging between 170 nm (in winter) and 225 nm (in summer) has been reported for station Alert between 2011 and 2013 (Sharma et al., 2017). More recently, a MMD at Alert was 216 nm in 2018 in winter and spring (Ohata et al., 2021), very similar to what was reported by Sharma et al. (2017). In Ny-Ålesund, in 2017, the MMD of 228 nm between February and March (Ohata et al., 2019).

The BC size distribution was additionally applied to validate the CAM5-ATRAS long-term global model simulations for Pallas, to better understand the uncertainties in modelled BC climate impacts in Arctic. In the BC size range from 65 to 537 nm the measured BC mass mean diameter (MmD) was 219 nm and the modelled BC MmD was 175 nm. Consistent with the observations, the modelled BC size distribution showed a limited temporal variability, within 10%. In contrast, the difference between the modelled and measured MmD size was higher, up to 25%.

Our findings suggest that, when modelling the climate impacts of BC in the Arctic, it is realistic to consider a BC size distribution with low variability. These results further imply that the BC coating must be very important for the climate impacts of BC in the Arctic compared to the BC core size itself, because the coating determines the amount of absorption enhancement in the atmosphere, impacts the BC's ability to act as cloud condensation nuclei (CCN), and ultimately determines the amount of BC wet deposition onto snow and ice.

Our study also provided new knowledge on the long-term stability of the SP2 in ambient measurements by comparison with a co-located COSMOS instrument. COSMOS has been shown an accuracy of 15% in the Arctic (Ohata et al., 2021b). In Pallas the M_{BC} measured by COSMOS and SP2 agreed to within about 6% throughout the year,

https://doi.org/10.5194/egusphere-2026-2102
Preprint. Discussion started: 27 April 2026

demonstrating the accuracy and stability of SP2 in long-term measurements. The long-term stability of the SP2 has not been reported in literature before.

Overall, our results help close gaps in the understanding of BC microphysical properties and their seasonal variability across the Arctic. This improved understanding is essential for improving BC representation in global models and for better constraining BC properties, leading to more reliable estimates of the BC climate effects in support of targeted climate and air-quality mitigation strategies.

Code availability

The code is available at https://github.com/ARM-DOE/PySP2

Data availability

The data will be made available on https://zenodo.org

Author contribution

JB, SO, YK conceived the study and wrote much of the paper. JB and SO did most of the data analysis. JS, EA and TM contributed to writing the manuscript and interpreting the results.

Competing interests

At least one of the (co-)authors is a member of the editorial board of Atmospheric Chemistry and Physics

Figures and Tables

https://doi.org/10.5194/egusphere-2026-2102
Preprint. Discussion started: 27 April 2026

Figure 1. Locations of the Arctic sites included in this study.

https://doi.org/10.5194/egusphere-2026-2102
Preprint. Discussion started: 27 April 2026

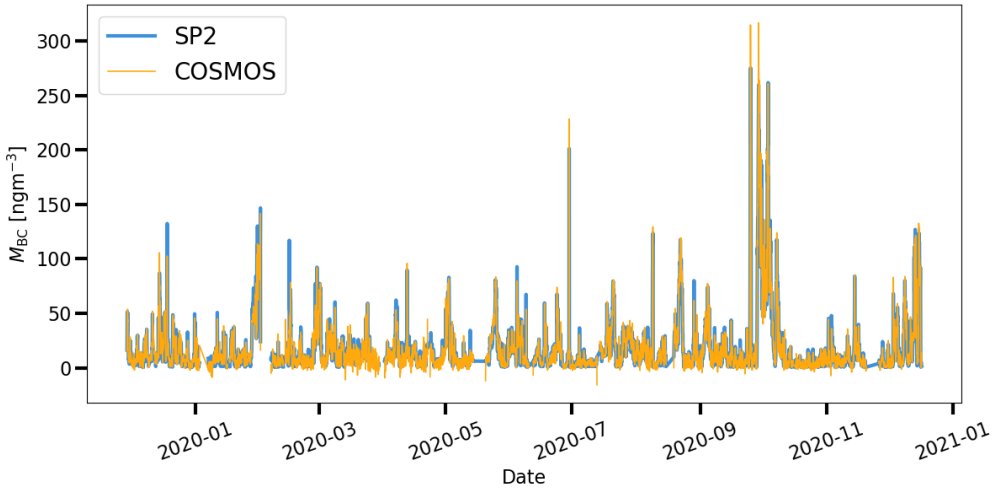

Figure 2. Time series of BC from the Single Particle Soot Photomerter (SP2) and BC from the COSMOS filter absorption photometer. Values are reported at STP conditions.

https://doi.org/10.5194/egusphere-2026-2102
Preprint. Discussion started: 27 April 2026

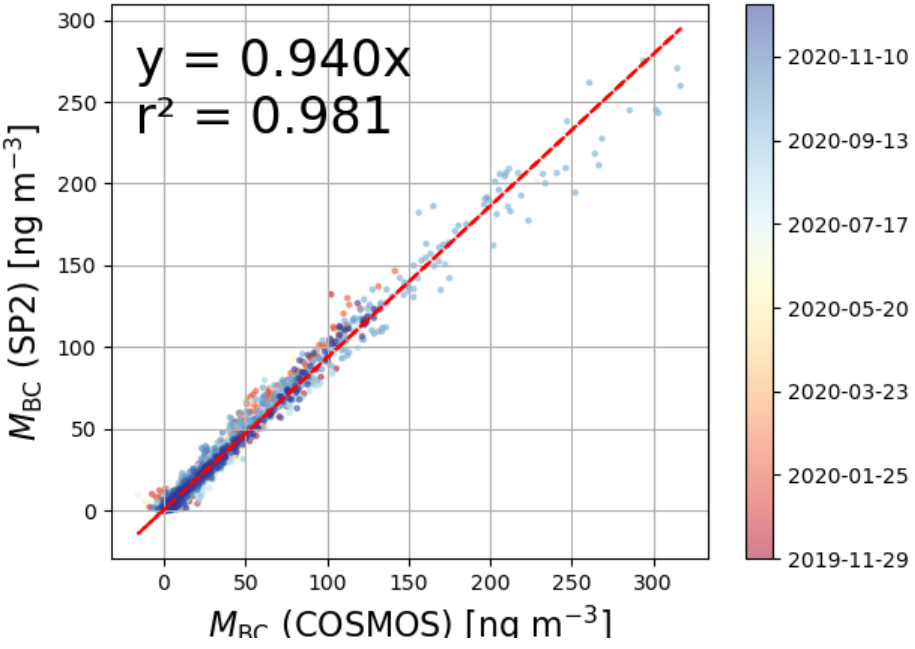

Figure 3. Scatter plot showing the correlation of M_{BC} measured with COSMOS (x-axis) and SP2 (y-axis) in units of ng m^{-3}. The colour bar shows the date of the data points. The curve fit has been forced to have an intercept of zero. r² is the Pearson correlation coefficient (r) squared.

https://doi.org/10.5194/egusphere-2026-2102
Preprint. Discussion started: 27 April 2026

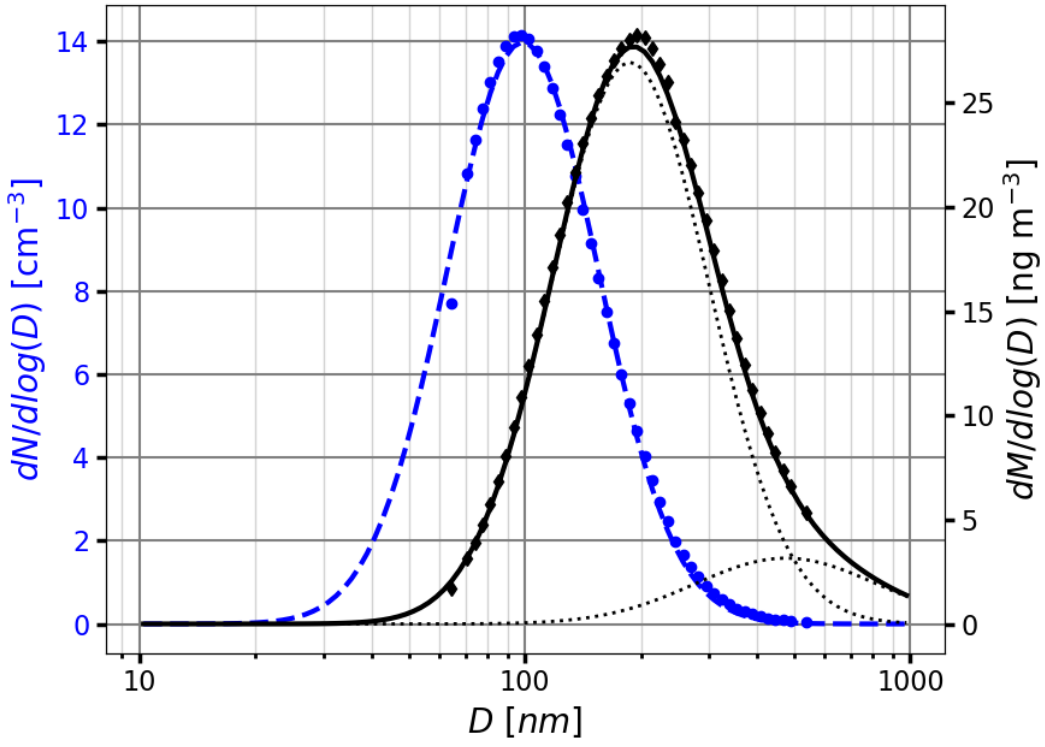

Figure 4. Mean number (blue dots and left y-axis) $n_n(D)$ and mass (black diamonds and right y-axis) $n_m(D)$ distributions of BC. The blue dashed and black solid lines show the log-normal fit to the size distribution data (dots). The CMD and MMD of the unimodal distributions are 99 nm and 195 nm, respectively. The σ_c and σ_m of the number, and mass size distributions are 1.57 and 1.66. The black dotted line shows the two modes fitted to the mass size distribution data. For the bimodal distribution, the smaller mode peaks at 187 nm (σ_m=1.60) and the larger mode peaks at 475 nm (σ_m=1.73).

https://doi.org/10.5194/egusphere-2026-2102
Preprint. Discussion started: 27 April 2026

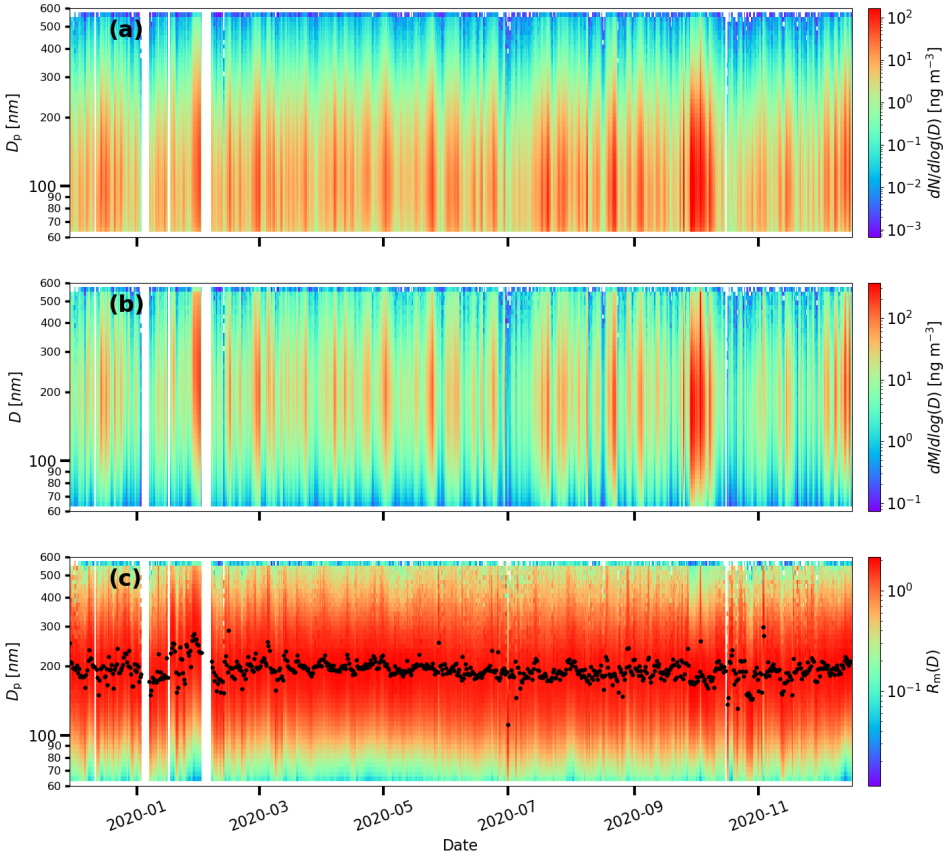

535

Figure 5. Time series of (a) BC number size distribution (dN/dlog(D)), (b) BC mass size distribution (dM/dlog(D)), and (c) normalized mass size distribution (R_m(D). In panel (c), the MMD of the size distribution is shown as black dots. The figure shows 12 h averages of data.

https://doi.org/10.5194/egusphere-2026-2102
Preprint. Discussion started: 27 April 2026

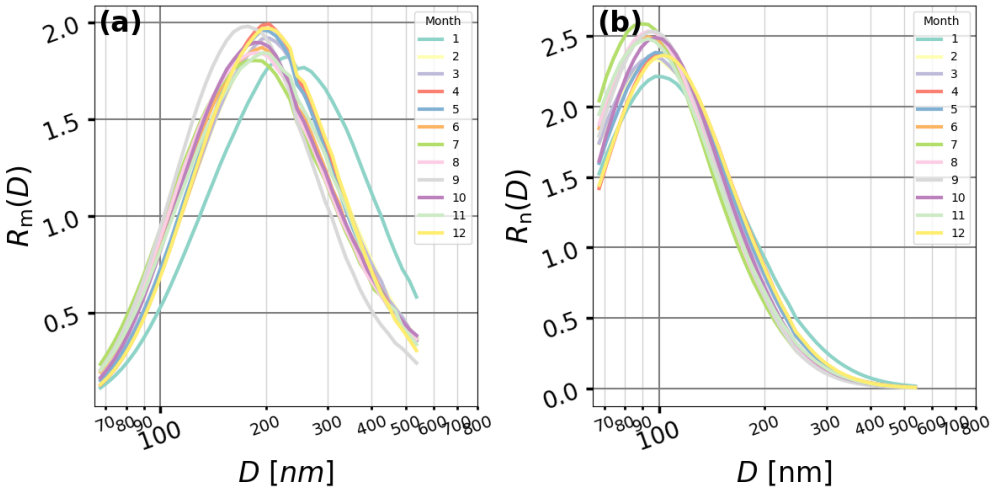

Figure 6. (a) Normalized mass distributions $R_m(D)$ and **(b)** normalized number distributions $R_n(D)$ of atmospheric BC for different months during the measurements period at Pallas. The legend in panel **(a)** and **(b)** shows the month of the year.

https://doi.org/10.5194/egusphere-2026-2102
Preprint. Discussion started: 27 April 2026

545

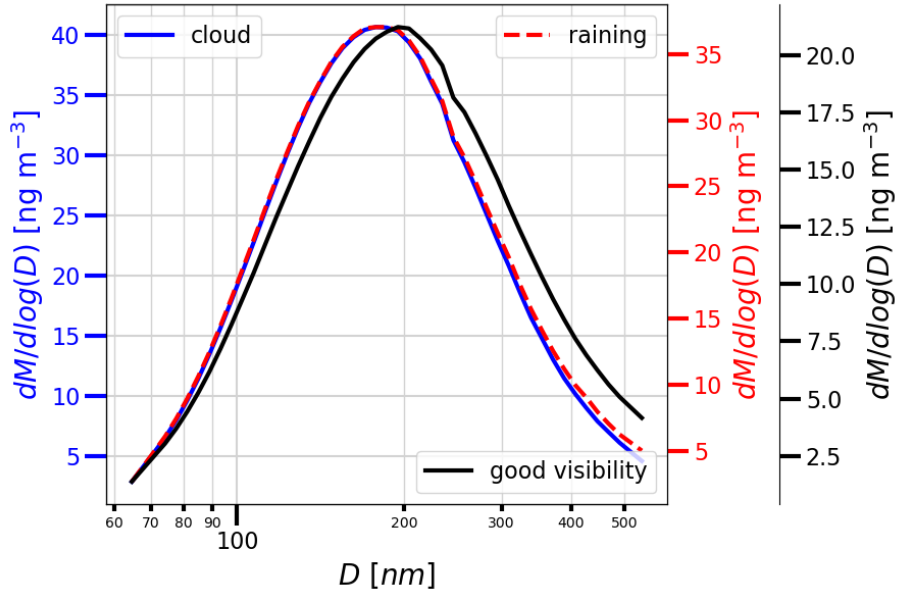

Figure 7. The figure shows BC mass size distributions when the station is inside clouds (blue, visibility < 500 m), when it is raining (red), and when the visibility at the station was good (black, visibility > 10 km).

https://doi.org/10.5194/egusphere-2026-2102
Preprint. Discussion started: 27 April 2026

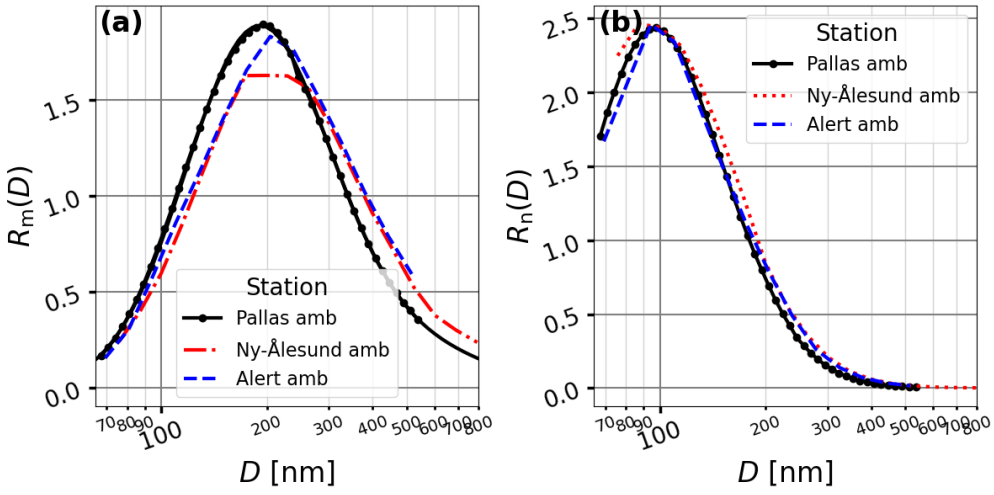

Figure 8. Panels **(a)** and **(b)** show the annual mean of $R_m(D)$ and $R_n(D)$ for Pallas, Ny-Ålesund and Alert. The data from Ny-Ålesund was obtained from February to March in 2017 (Ohata et al., 2019). The Alert data is from January to May 2018 (Ohata et al., 2021b).

https://doi.org/10.5194/egusphere-2026-2102
Preprint. Discussion started: 27 April 2026

555

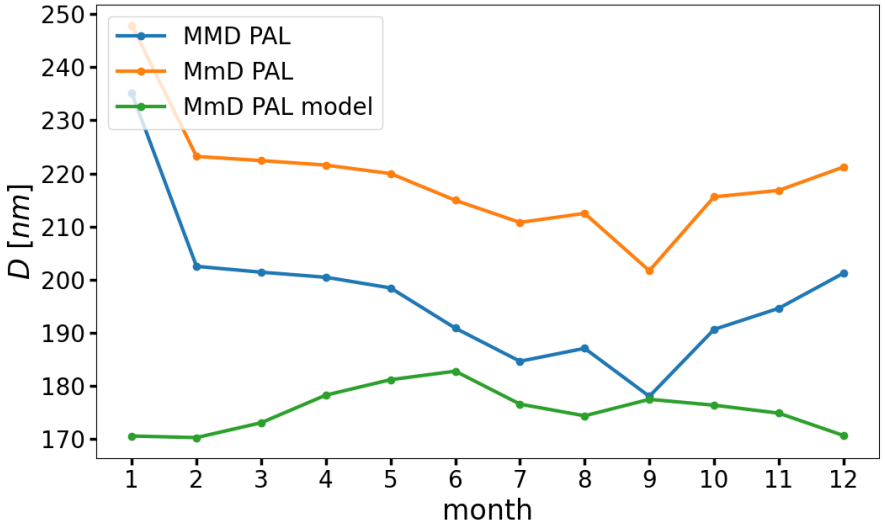

Figure 9. The monthly BC size distribution properties in Pallas (PAL). MMD (blue line) is the monthly mass median diameter calculated from data, MmD (yellow line) is the monthly mass mean diameter calculated from data and MmD (red line) is the mass median diameter from the model, with both model and measurements harmonized for the overlapping size range of 65-537 nm. Model results are labelled as "model" in the figure legend. The data shown in the figure is summarized in Table 1.

560

https://doi.org/10.5194/egusphere-2026-2102
Preprint. Discussion started: 27 April 2026

Table 1. Monthly statistics for the mass size distributions shown in Figures 6 and 8. The MMD is the mass median diameter, CMD is the count median diameter of the size distribution, σ_m is the width of $n_m(D)$, and σ_n is the width of $n_n(D)$. The mass mean diameter (MmD) and model mean diameter are calculated for the range of 65-537 nm which was the detection range of the SP2 at Pallas.

			Pallas			
Month	MMD [nm]	CMD [nm]	σ_m	σ_n	MmD model [nm]	MmD meas [nm]
1	235.1	102.0	1.72	1.67	170.6	247.9
2	202.5	97.4	1.66	1.63	170.3	223.2
3	201.4	96.9	1.66	1.63	173.1	222.4
4	200.5	104.3	1.62	1.57	178.3	221.6
5	198.5	100.5	1.64	1.59	181.2	220.0
6	190.9	94.0	1.68	1.59	182.8	215.0
7	184.7	89.7	1.71	1.59	176.6	210.8
8	187.1	93.7	1.69	1.58	174.4	212.5
9	178.1	96.2	1.61	1.55	177.5	201.7
10	190.7	99.2	1.66	1.56	176.4	215.6
11	194.6	91.8	1.69	1.62	174.9	216.8
12	201.2	104.2	1.62	1.58	170.7	221.2

Acknowledgements

Measurements at Pallas were supported by ACTRIS (Aerosol Clouds and Trace gases Research Infrastructure) and the Research Council of Finland (ACCC Flagship, nro 359342). This work was also supported by the Black and Brown Carbon in the Atmosphere and the Cryosphere project (BBrCAC project no. 341271). This work was also supported by the Japanese Ministry of Education, Culture, Sports, Science, and Technology (MEXT); Japan Society for the Promotion of Science KAKENHI Grant (JP20H00638, JP25K15423); the Arctic Challenge for Sustainability 3 (ArCS-3) (JPMXD1720251001); the Environment Research and Technology Development Fund (JPMEERF20232001) of the Environmental Restoration and Conservation Agency provided by Ministry of the Environment of Japan; and a grant for the Global

https://doi.org/10.5194/egusphere-2026-2102
Preprint. Discussion started: 27 April 2026

Environmental Research Coordination System from Ministry of the Environment of Japan (MLIT2253).

References

AMAP, 2021. AMAP Assessment 2021: Impacts of Short-lived Climate Forcers on Arctic Climate, Air Quality, and Human Health. Arctic Monitoring and Assessment Programme (AMAP), Tromsø, Norway. x + 375pp

Adachi, K., Chung, S. H., and Buseck, P. R.: Shapes of soot aerosol particles and implications for their effects on climate, J. Geophys. Res. Atmos., 115, https://doi.org/10.1029/2009JD012868, 2010.

Backman, J., Luoma, K., Servomaa, H., Vakkari, V., and Brus, D.: In-situ aerosol measurements at the Arctic Sammaltunturi measurement station during the Pallas Cloud Experiment 2022, https://doi.org/10.5194/essd-2025-284, 24 June 2025.

Baumgardner, D.: Warming of the Arctic lower stratosphere by light absorbing particles, Geophys. Res. Lett., 31, 10–13, https://doi.org/10.1029/2003GL018883, 2004.

Bond, T. C., Habib, G., and Bergstrom, R. W.: Limitations in the enhancement of visible light absorption due to mixing state, J. Geophys. Res. Atmos., 111, https://doi.org/10.1029/2006JD007315, 2006.

Bond, T. C., Doherty, S. J., Fahey, D. W., Forster, P. M., Berntsen, T., DeAngelo, B. J., Flanner, M. G., Ghan, S., Kärcher, B., Koch, D., Kinne, S., Kondo, Y., Quinn, P. K., Sarofim, M. C., Schultz, M. G., Schulz, M., Venkataraman, C., Zhang, H., Zhang, S., Bellouin, N., Guttikunda, S. K., Hopke, P. K., Jacobson, M. Z., Kaiser, J. W., Klimont, Z., Lohmann, U., Schwarz, J. P., Shindell, D., Storelvmo, T., Warren, S. G., and Zender, C. S.: Bounding the role of black carbon in the climate system: A scientific assessment, J. Geophys. Res. Atmos., 118, 5380–5552, https://doi.org/10.1002/jgrd.50171, 2013.

Fierce, L., Riemer, N., and Bond, T. C.: Explaining variance in black carbon's aging timescale, Atmos. Chem. Phys., 15, 3173–3191, https://doi.org/10.5194/acp-15-3173-2015, 2015.

Doulgeris, K. M., Kaikkonen, V., Juttula, H., Molkoselkä, E., Mäkynen, A., and Brus, D.: In situ surface cloud measurement dataset from four cloud spectrometers during the

https://doi.org/10.5194/egusphere-2026-2102
Preprint. Discussion started: 27 April 2026

Pallas Cloud Experiment (PaCE) 2022, Earth Syst. Sci. Data, 17, 6497–6506, https://doi.org/10.5194/essd-17-6497-2025, 2025.

Eckhardt, S., Quennehen, B., Olivié, D. J. L., Berntsen, T. K., Cherian, R., Christensen, J. H., Collins, W., Crepinsek, S., Daskalakis, N., Flanner, M., Herber, A., Heyes, C., Hodnebrog, Huang, L., Kanakidou, M., Klimont, Z., Langner, J., Law, K. S., Lund, M. T., Mahmood, R., Massling, A., Myriokefalitakis, S., Nielsen, I. E., Nøjgaard, J. K., Quaas, J., Quinn, P. K., Raut, J. C., Rumbold, S. T., Schulz, M., Sharma, S., Skeie, R. B., Skov, H., Uttal, T., Von Salzen, K., and Stohl, A.: Current model capabilities for simulating black carbon and sulfate concentrations in the Arctic atmosphere: A multi-model evaluation using a comprehensive measurement data set, Atmos. Chem. Phys., 15, 9413–9433, https://doi.org/10.5194/acp-15-9413-2015, 2015.

Fierce, L., Li, Y., Feng, Y., Riemer, N., Schutgens, N. A. J., Aiken, A. C., Dubey, M. K., Ma, P. L., and Wuebbles, D.: Constraining Black Carbon Aging in Global Models to Reflect Timescales for Internal Mixing, J. Adv. Model. Earth Syst., 17, https://doi.org/10.1029/2024MS004471, 2025.

Gysel, M., Laborde, M., Olfert, J. S., Subramanian, R., and Gréhn, A. J.: Effective density of Aquadag and fullerene soot black carbon reference materials used for SP2 calibration, Atmos. Meas. Tech., 4, 2851–2858, https://doi.org/10.5194/amt-4-2851-2011, 2011.

Hatakka, J., Aalto, T., Aaltonen, V., Aurela, M., Hakola, H., Komppula, M., Laurila, T., Lihavainen, H., Paatero, J., Salminen, K., and Viisanen, Y.: Overview of the atmospheric research activities and results at Pallas GAW station, Boreal Environ. Res., 8, 365–383, 2003.

Hoesly, R. M., Smith, S. J., Feng, L., Klimont, Z., Janssens-Maenhout, G., Pitkanen, T., Seibert, J. J., Vu, L., Andres, R. J., Bolt, R. M., Bond, T. C., Dawidowski, L., Kholod, N., Kurokawa, J. I., Li, M., Liu, L., Lu, Z., Moura, M. C. P., O'Rourke, P. R., and Zhang, Q.: Historical (1750-2014) anthropogenic emissions of reactive gases and aerosols from the Community Emissions Data System (CEDS), Geosci. Model Dev., 11, 369–408, https://doi.org/10.5194/gmd-11-369-2018, 2018.

Hussein, T., Dal Maso, M., Petäjä, T., Koponen, I. K., Paatero, P., Aalto, P. P., Hämeri, K., and Kulmala, M.: Evaluation of an automatic algorithm for fitting the particle number size distributions, Boreal Environ. Res., 10, 337–355, 2005.

https://doi.org/10.5194/egusphere-2026-2102
Preprint. Discussion started: 27 April 2026

Jacobson, M. Z.: Strong radiative heating due to the mixing state of black carbon in atmospheric aerosols., Nature, 409, 695–7, https://doi.org/10.1038/35055518, 2001.

Jurányi, Z., Zanatta, M., Lund, M. T., Samset, B. H., Skeie, R. B., Sharma, S., Wendisch, M., and Herber, A.: Atmospheric concentrations of black carbon are substantially higher in spring than summer in the Arctic, Commun. Earth Environ., 4, https://doi.org/10.1038/s43247-023-00749-x, 2023.

Koch, D., Schulz, M., Kinne, S., Mcnaughton, C., Spackman, J. R., Balkanski, Y., Bauer, S., Berntsen, T., Bond, T. C., Boucher, O., Penner, J. E., Perlwitz, J., Pitari, G., Reddy, S., Sahu, L., Sakamoto, H., Schuster, G., Schwarz, J. P., Seland, Ø., Stier, P., Takegawa, N., Takemura, T., Textor, C., Van Aardenne, J. A., and Zhao, Y.: Evaluation of black carbon estimations in global aerosol models, Atmos. Chem. Phys, 28 pp., 2009.

Kondo, Y.: Effects of Black Carbon on Climate: Advances in Measurement and Modeling, Monogr. Environ. Earth Planets, 3, 1–85, https://doi.org/10.5047/meep.2015.00301.0001, 2015.

Kondo, Y., Sahu, L., Kuwata, M., Miyazaki, Y., Takegawa, N., Moteki, N., Imaru, J., Han, S., Nakayama, T., Oanh, N. T. K., Hu, M., Kim, Y. J., and Kita, K.: Stabilization of the mass absorption cross section of black carbon for filter-based absorption photometry by the use of a heated inlet, Aerosol Sci. Tech., 43, 741–756, https://doi.org/10.1080/02786820902889879, 2009.

Kondo, Y., Sahu, L., Moteki, N., Khan, F., Takegawa, N., Liu, X., Koike, M., and Miyakawa, T.: Consistency and traceability of black carbon measurements made by laser-induced incandescence, thermal-optical transmittance, and filter-based photo-absorption techniques, Aerosol Sci. Tech., 45, 295–312, https://doi.org/10.1080/02786826.2010.533215, 2011.

Laborde, M., Mertes, P., Zieger, P., Dommen, J., Baltensperger, U., and Gysel, M.: Sensitivity of the Single Particle Soot Photometer to different black carbon types, Atmos. Meas. Tech., 5, 1031–1043, https://doi.org/10.5194/amt-5-1031-2012, 2012.

Matsui, H.: Development of a global aerosol model using a two-dimensional sectional method: 1. Model design, J. Adv. Model. Earth Syst., 9, 1921–1947, https://doi.org/10.1002/2017MS000936, 2017.

https://doi.org/10.5194/egusphere-2026-2102
Preprint. Discussion started: 27 April 2026

Matsui, H. and Mahowald, N.: Development of a global aerosol model using a two-dimensional sectional method: 2. Evaluation and sensitivity simulations, J. Adv. Model. Earth Syst., 9, 1887–1920, https://doi.org/10.1002/2017MS000937, 2017.

Matsui, H., Hamilton, D. S., and Mahowald, N. M.: Black carbon radiative effects highly sensitive to emitted particle size when resolving mixing-state diversity, Nat. Commun., 9, 1–11, https://doi.org/10.1038/s41467-018-05635-1, 2018.

Matsui, H., Mori, T., Ohata, S., Moteki, N., Oshima, N., Goto-Azuma, K., Koike, M., and Kondo, Y.: Contrasting source contributions of Arctic black carbon to atmospheric concentrations, deposition flux, and atmospheric and snow radiative effects, Atmos. Chem. Phys., 22, 8989–9009, https://doi.org/10.5194/acp-22-8989-2022, 2022.

Mikhailov, E. F., Vlasenko, S. S., Podgorny, I. a., Ramanathan, V., and Corrigan, C. E.: Optical properties of soot–water drop agglomerates: An experimental study, J. Geophys. Res., 111, D07209, https://doi.org/10.1029/2005JD006389, 2006.

Miyazaki, Y., Kondo, Y., Sahu, L. K., Imaru, J., Fukushima, N., and Kano, M.: Performance of a newly designed continuous soot monitoring system (COSMOS), J. Environ. Monitor., 10, 1195, https://doi.org/10.1039/b806957c, 2008.

Mori, T., Ohata, S., Kondo, Y., Oshima, N., Moteki, N., Hayakawa, Y., Tobo, Y., Sinha, P. R., Aggarwal, S. G., Malik, A., and Koike, M.: Derivation of the correction factors needed for COSMOS observations at high mass concentrations of black carbon, Aerosol Sci. Tech., 59, 1082–1094, https://doi.org/10.1080/02786826.2025.2499690, 2025.

Ohata, S., Kondo, Y., Moteki, N., Mori, T., Yoshida, A., Sinha, P. R., and Koike, M.: Accuracy of black carbon measurements by a filter-based absorption photometer with a heated inlet, Aerosol Sci. Tech., 53, 1079–1091, https://doi.org/10.1080/02786826.2019.1627283, 2019.

Ohata, S., Koike, M., Yoshida, A., Moteki, N., Adachi, K., Oshima, N., Matsui, H., Eppers, O., Bozem, H., Zanatta, M., and Herber, A. B.: Arctic black carbon during PAMARCMiP 2018 and previous aircraft experiments in spring, Atmos. Chem. Phys., 21, 15861–15881, https://doi.org/10.5194/acp-21-15861-2021, 2021a.

Ohata, S., Mori, T., Kondo, Y., Sharma, S., Hyvärinen, A., Andrews, E., Tunved, P., Asmi, E., Backman, J., Servomaa, H., Veber, D., Eleftheriadis, K., Vratolis, S., Krejci, R., Zieger, P., Koike, M., Kanaya, Y., Yoshida, A., Moteki, N., Zhao, Y., Tobo, Y., Matsushita, J., and Oshima, N.: Estimates of mass absorption cross sections of black

https://doi.org/10.5194/egusphere-2026-2102
Preprint. Discussion started: 27 April 2026

carbon for filter-based absorption photometers in the Arctic, Atmos. Meas. Tech., 14, 6723–6748, https://doi.org/10.5194/amt-14-6723-2021, 2021b.

Oshima, N., Yukimoto, S., Deushi, M., Koshiro, T., Kawai, H., Tanaka, T. Y., and Yoshida, K.: Global and Arctic effective radiative forcing of anthropogenic gases and aerosols in MRI-ESM2.0, Prog. Earth Planet. Sci., 7, https://doi.org/10.1186/s40645-020-00348-w, 2020.

Petzold, A., Ogren, J. a., Fiebig, M., Laj, P., Li, S. M., Baltensperger, U., Holzer-Popp, T., Kinne, S., Pappalardo, G., Sugimoto, N., Wehrli, C., Wiedensohler, A., and Zhang, X. Y.: Recommendations for reporting black carbon measurements, Atmos. Chem. Phys., 13, 8365–8379, https://doi.org/10.5194/acp-13-8365-2013, 2013.

Quinn, P. K., Shaw, G., Andrews, E., Dutton, E. G., Ruoho-Airola, T., and Gong, S. L.: Arctic haze: current trends and knowledge gaps, Tellus B: Chem. Phys. Meteorol., 59, 99, https://doi.org/10.1111/j.1600-0889.2006.00236.x, 2007.

Raatikainen, T., Brus, D., Hyvärinen, A. P., Svensson, J., Asmi, E., and Lihavainen, H.: Black carbon concentrations and mixing state in the Finnish Arctic, Atmos. Chem. Phys., 15, 10057–10070, https://doi.org/10.5194/acp-15-10057-2015, 2015.

Rantanen, M., Karpechko, A. Y., Lipponen, A., Nordling, K., Hyvärinen, O., Ruosteenoja, K., Vihma, T., and Laaksonen, A.: The Arctic has warmed nearly four times faster than the globe since 1979, Commun. Earth Environ., 3, https://doi.org/10.1038/s43247-022-00498-3, 2022.

Sand, M., Berntsen, T. K., von Salzen, K., Flanner, M. G., Langner, J., and Victor, D. G.: Response of Arctic temperature to changes in emissions of short-lived climate forcers, Nat. Clim. Chang., 6, 286–289, https://doi.org/10.1038/nclimate2880, 2016.

Schmale, J., Sharma, S., Decesari, S., Pernov, J., Massling, A., Hansson, H. C., Von Salzen, K., Skov, H., Andrews, E., Quinn, P. K., Upchurch, L. M., Eleftheriadis, K., Traversi, R., Gilardoni, S., Mazzola, M., Laing, J., and Hopke, P.: Pan-Arctic seasonal cycles and long-term trends of aerosol properties from 10 observatories, Atmos. Chem. Phys., 22, 3067–3096, https://doi.org/10.5194/acp-22-3067-2022, 2022.

Schmeisser, L., Backman, J., Ogren, J. A., Andrews, E., Asmi, E., Starkweather, S., Uttal, T., Fiebig, M., Sharma, S., Eleftheriadis, K., Vratolis, S., Bergin, M., Tunved, P., and Jefferson, A.: Seasonality of aerosol optical properties in the Arctic, Atmos. Chem. Phys., 18, 11599–11622, https://doi.org/10.5194/acp-18-11599-2018, 2018.

https://doi.org/10.5194/egusphere-2026-2102
Preprint. Discussion started: 27 April 2026

Schulz, H., Zanatta, M., Bozem, H., Richard Leaitch, W., Herber, A. B., Burkart, J., Willis, M. D., Kunkel, D., Hoor, P. M., Abbatt, J. P. D., and Gerdes, R.: High Arctic aircraft measurements characterising black carbon vertical variability in spring and summer, Atmos. Chem. Phys., 19, 2361–2384, https://doi.org/10.5194/acp-19-2361-2019, 2019.

Schwarz, J. P., Gao, R. S., Fahey, D. W., Thomson, D. S., Watts, L. A., Wilson, J. C., Reeves, J. M., Darbeheshti, M., Baumgardner, D. G., Kok, G. L., Chung, S. H., Schulz, M., Hendricks, J., Lauer, A., K??rcher, B., Slowik, J. G., Rosenlof, K. H., Thompson, T. L., Langford, A. O., Loewenstein, M., and Aikin, K. C.: Single-particle measurements of midlatitude black carbon and light-scattering aerosols from the boundary layer to the lower stratosphere, J. Geophys. Res. Atmos., 111, 1–15, https://doi.org/10.1029/2006JD007076, 2006.

Schwarz, J. P., Spackman, J. R., Gao, R. S., Watts, L. A., Stier, P., Schulz, M., Davis, S. M., Wofsy, S. C., and Fahey, D. W.: Global-scale black carbon profiles observed in the remote atmosphere and compared to models, Geophys. Res. Lett., 37, 1–5, https://doi.org/10.1029/2010GL044372, 2010a.

Schwarz, J. P., Spackman, J. R., Gao, R. S., Perring, a. E., Cross, E., Onasch, T. B., Ahern, a., Wrobel, W., Davidovits, P., Olfert, J., Dubey, M. K., Mazzoleni, C., and Fahey, D. W.: The Detection Efficiency of the Single Particle Soot Photometer, Aerosol Sci. Tech., 44, 612–628, https://doi.org/10.1080/02786826.2010.481298, 2010b.

Schwarz, J. P., Katich, J. M., Lee, S. L., Thomson, D. S., and Watts, L. A.: "Invisible bias" in the single particle soot photometer due to trigger deadtime, Aerosol Sci. Tech., 56, 623–635, https://doi.org/10.1080/02786826.2022.2064265, 2022.

Sharma, S., Richard Leaitch, W., Huang, L., Veber, D., Kolonjari, F., Zhang, W., Hanna, S. J., Bertram, A. K., and Ogren, J. A.: An evaluation of three methods for measuring black carbon in Alert, Canada, Atmos. Chem. Phys., 17, 15225–15243, https://doi.org/10.5194/acp-17-15225-2017, 2017.

Stephens, M., Turner, N., and Sandberg, J.: Particle identification by laser-induced incandescence in a solid-state laser cavity., Appl. Opt., 42, 3726–36, 2003.

Stohl, A.: Characteristics of atmospheric transport into the Arctic troposphere, J. Geophys. Res., 111, D11306, https://doi.org/10.1029/2005JD006888, 2006.

https://doi.org/10.5194/egusphere-2026-2102
Preprint. Discussion started: 27 April 2026

van der Werf, G. R., Randerson, J. T., Giglio, L., van Leeuwen, T. T., Chen, Y., Rogers, B. M., Mu, M., van Marle, M. J. E., Morton, D. C., Collatz, G. J., Yokelson, R. J., and Kasibhatla, P. S.: Global fire emissions estimates during 1997–2016, Earth Syst. Sci. Data, 9, 697–720, https://doi.org/10.5194/essd-9-697-2017, 2017.

Whaley, C. H., Mahmood, R., Von Salzen, K., Winter, B., Eckhardt, S., Arnold, S., Beagley, S., Becagli, S., Chien, R. Y., Christensen, J., Damani, S. M., Dong, X., Eleftheriadis, K., Evangeliou, N., Faluvegi, G., Flanner, M., Fu, J. S., Gauss, M., Giardi, F., Gong, W., Hjorth, J. L., Huang, L., Im, U., Kanaya, Y., Krishnan, S., Klimont, Z., Kühn, T., Langner, J., Law, K. S., Marelle, L., Massling, A., Olivié, D., Onishi, T., Oshima, N., Peng, Y., Plummer, D. A., Popovicheva, O., Pozzoli, L., Raut, J. C., Sand, M., Saunders, L. N., Schmale, J., Sharma, S., Skeie, R. B., Skov, H., Taketani, F., Thomas, M. A., Traversi, R., Tsigaridis, K., Tsyro, S., Turnock, S., Vitale, V., Walker, K. A., Wang, M., Watson-Parris, D., and Weiss-Gibbons, T.: Model evaluation of short-lived climate forcers for the Arctic Monitoring and Assessment Programme: A multi-species, multi-model study, Atmos. Chem. Phys., 22, 5775–5828, https://doi.org/10.5194/acp-22-5775-2022, 2022.

Zanatta, M., Laj, P., Gysel, M., Baltensperger, U., Vratolis, S., and Eleftheriadis, K.: Effects of mixing state on optical and radiative properties of black carbon in the European Arctic, Atmos. Chem. Phys, 18, 14037–14057, https://doi.org/10.5194/acp-18-14037-2018, 2018.

Zanatta, M., Mertes, S., Jourdan, O., Dupuy, R., Järvinen, E., Schnaiter, M., Eppers, O., Schneider, J., Jurányi, Z., and Herber, A.: Airborne investigation of black carbon interaction with low-level, persistent, mixed-phase clouds in the Arctic summer, Atmos. Chem. Phys., 23, 7955–7973, https://doi.org/10.5194/acp-23-7955-2023, 2023.

Zhao, N., Dong, X., Huang, K., Fu, J. S., Lund, M. T., Sudo, K., Henze, D., Kucsera, T., Lam, Y. F., Chin, M., and Tilmes, S.: Responses of Arctic black carbon and surface temperature to multi-region emission reductions: A Hemispheric Transport of Air Pollution Phase 2 (HTAP2) ensemble modeling study, Atmos. Chem. Phys., 21, 8637–8654, https://doi.org/10.5194/acp-21-8637-2021, 2021.